Nuclear Science and Techniques (2026) 37:134
https://doi.org/10.1007/s41365-026-01958-7

Ab initio study of vacancy aggregation in solute clusters in reactor pressure vessel materials

Zhao-Yang Yu[1] · Shi-Hua Qiao[1] · Liang Chen[1] · Yao Shen[2] · Ling-Ti Kong[2] · Zheng-Cao Li[3]

Received: 30 June 2024 / Revised: 18 November 2024 / Accepted: 20 December 2024 / Published online: 12 May 2026

Abstract
Developing an irradiation embrittlement predictive model for low-Cu reactor pressure vessel steels is essential for extending the life of modern pressurized water reactors. Irradiation-produced dislocation loops are recognized as the leading causes of embrittlement, surpassing the mechanism of Cu clustering with a reduction in Cu content in modern steels. Extensive data have been accumulated from surveillance programs on high-Cu steels used in old reactors. The extrapolation of these data to low-Cu systems for embrittlement prediction requires a comprehensive understanding of the interactions between Cu, particularly Cu-rich clusters, and radiation defects. Therefore, in this study, ab initio calculations of vacancy aggregation in solute clusters containing Cu, Ni, Mn, and Si were performed. The interactions between the solute elements and vacancies in the solute clusters and Fe matrix were analyzed. The results demonstrated the occurrence of attractive interactions between the Cu clusters and vacancies. The addition of Si and the synergistic effect between Ni and Mn facilitated vacancy aggregation in the solute clusters. The behavior of Mn correlated with its magnetic state, and the size effects of the solute elements were analyzed.

Keywords Ab initio calculations · Irradiation embrittlement · Solute clusters · Radiation defects · Reactor pressure vessel

1 Introduction

Pressurized water reactors (PWR) are a mainstream reactor type in service worldwide and serve as safe and economical energy sources for carbon neutrality. Nuclear structural materials used in reactor pressure vessels (RPVs) are exposed to intense neutron irradiation, at energies of the order of MeV, for long-term service, resulting in the irradiation embrittlement of RPV steels [1–4]. Developing an irradiation embrittlement predictive model based on physical mechanisms is crucial to predict the long-term integrity of RPV steels using irradiation surveillance data obtained from steels with various material variables and irradiation conditions. However, to construct such a model, understanding the physics of microstructural evolution is important. Three microstructural features have been identified as contributors to irradiation embrittlement: solute clusters, dislocation loops, and phosphorus (P) grain-boundary segregation [1, 5–8].

Cu is one of the main constituents of solute clusters owing to its low solubility limit (approximately 0.003%) in body-centered cubic (bcc) Fe at RPV service temperatures [9, 10]. Cu-rich clusters can act as obstacles to dislocation movement, resulting in irradiation embrittlement [11–13]. Benefiting from the understanding that Cu is a harmful element, the Cu content has been greatly reduced (lower than 0.1%) in modern RPV steels [14]. For low-Cu RPV steels, irradiation-induced dislocation loops are the leading cause of embrittlement, surpassing the mechanism of Cu clustering [15–17]. Aiming to evaluate the effect of Cu on dislocation loop formation, Hernández-Mayoral et al. [18]

This work was supported by the National Natural Science Foundation of China (No. 12205188), Natural Science Foundation of Shanghai (No. 22ZR1428700), and China National Nuclear Corporation (No. CNNC-LCKY-202236).

✉ Liang Chen
liang.chen@sjtu.edu.cn

[1] SJTU Paris Elite Institute of Technology, Shanghai Jiao Tong University, Shanghai 200240, China

[2] School of Materials Science and Engineering, Shanghai Jiao Tong University, Shanghai 200240, China

[3] School of Materials Science and Engineering, Tsinghua University, Beijing 100084, China

utilized transmission electron microscopy and analyzed the dislocation loops formed under neutron irradiation in Fe and Fe-Cu alloys. The results showed that the dislocation loops in Fe-Cu were smaller in size owing to the formation of Cu-vacancy complexes, which enhanced the recombination of interstitials and vacancies at the Cu-vacancy sites, decreased the concentration of interstitials, and inhibited the growth of dislocation loops. Arokiam et al. [19, 20] used molecular statics and performed molecular dynamics (MD) calculations, revealing that in bcc Fe, pure Cu clusters and vacancies attract each other, whereas the pure Cu clusters and interstitial clusters repulse each other over a long range but attract over a short range. The Cu clusters could act as sinks for defects and recombination centers for vacancies and interstitials. Notably, irradiation surveillance databases contain large amounts of data obtained from old steels with high Cu contents (higher than 0.15%) [14, 21]. The Cu-rich clusters formed under irradiation can trap defects, thereby contributing to the reduced embrittlement caused by the dislocation loops originating from defect growth in high-Cu steels; such a phenomenon is not observed in low-Cu steels. Neglecting this factor leads to the underestimation of the irradiation embrittlement of low-Cu steels predicted by the prediction models, which poses a potential risk to the safe operation of nuclear power plants.

Although Cu is recognized as a main element in solute clusters, these clusters also contain Fe, Ni, Mn, and Si [22–25]. For the interactions between Ni, Mn, and vacancies, based on ab initio calculations, Vincent et al. [26] noticed an attraction between Ni and vacancies, and Olsson et al. [27] found that Mn could attract vacancies due to its antiferromagnetic state. Using positron annihilation spectroscopy (PAS), Nagai et al. [28] observed the formation of Ni-vacancy complexes in Fe-Ni alloys and Mn-vacancy complexes in Fe-Mn alloys under electron irradiation, and Chen et al. [29] also indicated the formation of Mn-vacancy complexes under ion irradiation. These data highlight the need to investigate the influences of Ni, Mn, and Si on the interactions between Cu-rich clusters and radiation defects.

In this study, ab initio calculations based on the density functional theory were performed to investigate vacancy aggregation in solute clusters containing Cu, Ni, Mn, and Si in bcc Fe. The interactions between the solute elements and vacancies in the solute clusters and Fe matrix were simulated. The behavior of vacancy aggregation from the matrix to the solute cluster and the effects of solute elements, including Cu, Ni, Mn, and Si, were examined. Detailed analyses of these interactions were performed. Finally, conclusions are presented.

2 Method

This study utilized the Vienna Ab initio Simulation Package (VASP) to investigate defects in RPV steels. The simulation parameters are consistent with those used in a previous study [30]. VASP calculations were performed on a plane-wave basis, employing pseudopotentials developed within the projector augmented wave (PAW) method, and the Perdew–Burke–Ernzerhof (PBE) [31] exchange-correlation functional of the spin-polarized generalized gradient approximation (GGA) was applied. The pseudopotentials were obtained from the VASP Library version 5.3.2. Brillouin zone sampling was performed using the Monkhorst-Pack scheme.

A $3 \times 3 \times 3$ k-point mesh was chosen in accordance with the convergence tests, and the plane-wave cutoff energy was set to 300 eV, which is consistent with previous studies [27, 30, 32, 33]. Simulations were performed on a 128-atom bcc supercell with periodic boundary conditions matching the bcc structure of the Fe matrix in RPV steels. For Cu-rich clusters, this is justified by the coherence between these clusters and the Fe matrix because of the small size (diameter of $2-4$ nm) of such clusters in RPV steels [34]. Cu clusters in α-Fe maintain a coherent bcc structure up to a diameter of approximately 6.5 nm at 290 °C [35]. This bcc supercell model setting has also been used in previous ab initio studies [36, 37] to investigate the segregation of solute atoms at the interface between Cu-rich clusters and Fe matrix. Defect energy calculations were performed at a constant volume using an equilibrium lattice parameter of 0.2866 nm for bcc Fe.

For the investigated system, the binding energy E_b between n objects $X_i(i = 1, 2, .., n)$ (which represents solute atoms or vacancies) is calculated as follows:

$$E_b(X_1, X_2, ..., X_n) = \sum_{i=1,...,n} E(X_i) - [E(\sum_{i=1,...,n} X_i) + (n-1)E_{ref}]. \quad (1)$$

In this scheme, $E(X_i)$ describes the energy of a supercell with only one defect, $E(\sum_{i=1,...,n} X_i)$ represents the energy of a supercell containing all defects, E_{ref} represents the energy of a perfect supercell with no defects. This equation represents the energy difference between the system in which all defects interact with each other and the system with no interactions among the defects, and was applied in a previous study. According to this definition, a positive binding energy indicates an attractive interaction between the defects and a stable system.

The vacancy formation energy for a supercell containing n solute atoms, $Y_i(i = 1, 2, ..., n)$, is calculated as follows:

$$E_f(Y_1, Y_2, ..., Y_n) = E(\sum_{i=1,...,n} Y_i + V) - [E(\sum_{i=1,...,n} Y_i) - \frac{1}{N} E_{ref}], \quad (2)$$

where V is the vacancy, $E(\sum_{i=1,...,n} Y_i + V)$ is the energy of the supercell containing the solute atoms and one vacancy V, $E(\sum_{i=1,...,n} Y_i)$ is the energy of the supercell with all solute atoms, N is the number of atom sites in the 128-atom supercell, and E_{ref} denotes the energy of a perfect supercell devoid of defects. This equation, representing the energy difference before and after vacancy formation, is developed based on the vacancy formation energy model used in a previous study [38]. A positive value indicates that energy is required for the formation of vacancies in the lattice.

3 Results

3.1 Ab initio results for the solute cluster

Using the coherent bcc supercell model constructed for the Cu-rich clusters as described in Sect. 2, the interaction between Ni/Mn/Si and the vacancies in the Cu-rich clusters was investigated. The primary parameter was the vacancy formation energy in the different solute-atom environments. Table 1 lists the values calculated for the Cu and Fe matrices. The vacancy formation energy for α-Fe, calculated in this study, was 2.27 eV, which agreed well with that obtained from previous calculations [38–41]. The vacancy formation energy was significantly lower in the Cu cluster (0.73 eV), consistent with that obtained using a 128-atom bcc Cu supercell in a previous study [38] and with that at the center of a 15-atom bcc Cu cluster calculated by Sato et al. [42]. From a thermodynamic perspective, these data suggest that vacancies are preferentially located in Cu clusters rather than in the Fe matrix.

In this study, the solute cluster was first constructed by replacing two Cu atoms with one solute atom (Ni, Mn, or Si) and one vacancy. In this configuration, the distance between the solute atom and vacancy varied from the first nearest neighbor (1nn) to the fifth nearest neighbor (5nn), as shown in Fig. 1. The vacancy formation energies of solute clusters are shown in Fig. 2. Among all the solute clusters, the vacancy formation energy was significantly lower in the Cu-Si cluster than in the pure Cu cluster. The energy values were 0.60 eV and 0.58 eV when the Si vacancy distances were 1nn and 2nn, respectively. The energy values approached that in the pure Cu cluster (0.73 eV) when the distance was larger than 3nn. These results indicate that Si favors vacancy positioning in the solute cluster and that this effect is short-range. The 1nn vacancy formation energy in the Cu-Ni cluster is almost 0.07 eV higher than that in the pure Cu cluster. This suggests that Ni may slightly impede vacancy siting in the solute clusters. For Mn, the vacancy-formation energies indicate that Mn might weakly suppress vacancies in the solute cluster at 2nn. In conclusion, the single effects of both Ni and Mn on vacancy positioning in the cluster are weak. Figure 3 shows the binding energies between the solute atoms and vacancies in the solute clusters. These data are consistent with the calculated vacancy formation energies; an attractive interaction between solute atoms and vacancies corresponds to a lower vacancy formation energy in the solute cluster.

Considering the enriched contents of Ni, Mn, and Si in the solute clusters compared to the Fe matrix, the effects of increasing the solute atoms in the solute clusters were also investigated. The supercells were constructed by replacing the three Cu atoms with two solute atoms (Ni, Mn, or Si) and one vacancy. This configuration is illustrated in Fig. 1, where the two solute atoms are at 1nn of the vacancy, considering their short-range interaction, and the distances between the two solute atoms are 2nn, 3nn, and 5nn. Figure 4 shows the vacancy formation energies of the solute clusters. The vacancy formation energies in the Cu-2Si and Cu-2Mn clusters were lower than the 1nn values for the Cu-Si and Cu-Mn clusters, respectively. Additionally, the vacancy formation energy in the Cu-2Ni cluster was higher than that in the Cu-Ni cluster. Therefore, increasing the concentration of solute atoms enhanced the effects of Ni, Mn, and Si at 1nn of the vacancy on the positioning of vacancies within the solute clusters. This observation highlights the pronounced effect of Si addition, in contrast to the relatively minor impact of Ni and Mn additions.

The introduction of solute atoms and vacancies into the simulated supercell disrupted the local atomic arrangement, leading to lattice distortion. The lattice distortion is calculated as follows:

$$D_{matrix} = \sum_i |d_i|, \quad (3)$$

where $|d_i|$ is the absolute value of the displacement of the matrix atom i and is calculated by comparing the supercell before and after relaxation. The lattice distortion caused by one solute atom and one vacancy in the solute clusters is shown in Fig. 5. D_{matrix} caused by Ni and vacancies, or by Mn and vacancies, is consistent with that caused by one vacancy in the pure Cu cluster, indicating that single Ni or Mn atoms minimize lattice distortion. Thus, if only the size effect is considered, then Si is expected to exhibit the highest vacancy formation energy. The presence of a vacancy in the lattice creates a traction zone, which is expected to constitute a preferential site for oversized atoms; the lowest binding energy should be between those of Si and the

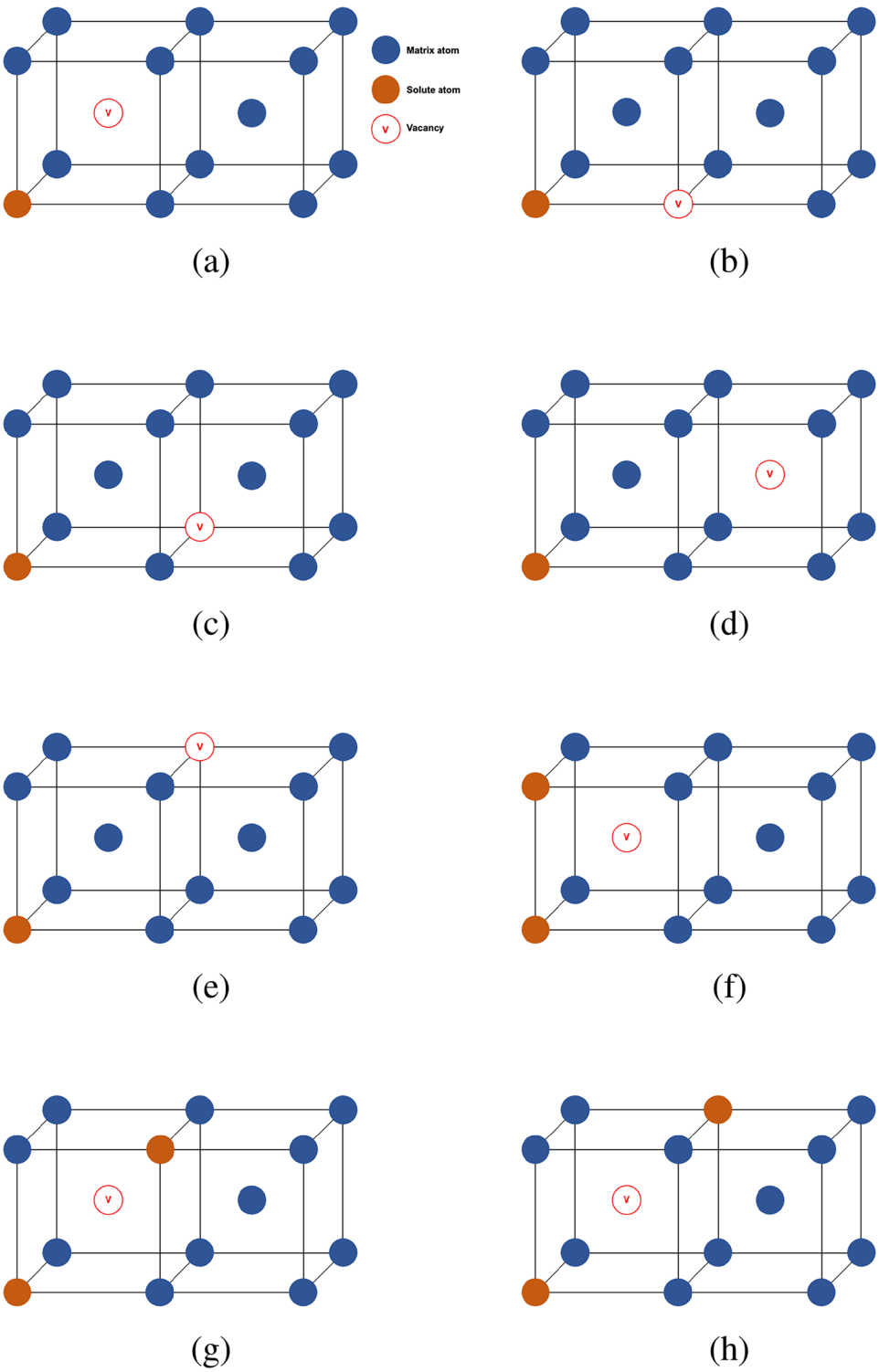

Fig. 1 (Color online) Configuration of the bcc supercell containing (a)–(e) one solute atom and one vacancy, and (f)–(h) two solute atoms and one vacancy. The matrix atoms are in blue, and the solute atom is in purple. Specifically, the configurations are: 1nn solute atom–vacancy (a), 2nn solute atom–vacancy (b), 3nn solute atom–vacancy (c), 4nn solute atom–vacancy (d), 5nn solute atom–vacancy (e), 2nn solute atom–solute atom and nearby vacancy (f), 3nn solute atom–solute atom and nearby vacancy (g), and 5nn solute atom–solute atom and nearby vacancy (h)

vacancy. Thus, analyzing the size effect is not sufficient for understanding the interactions between solute atoms and vacancies; in addition, the contribution of chemical interactions is non-negligible. Systematic analyses were conducted on surveillance specimens from Japanese PWRs [43, 44]. The mean atomic compositions of the clusters were 6Cu-10Ni-6Mn-7Si, 2Cu-11Ni-5Mn-9Si, and 0Cu-12Ni-6Mn-12Si for the 0.12 wt% Cu, 0.07 wt% Cu, and 0.04 wt% Cu steels, respectively. In the clusters, the Si concentration increased as the Cu concentration decreased, whereas the Ni and Mn concentrations remained unchanged, indicating a negative interaction between Si and Cu. This result is

Table 1 Vacancy formation energies in the 128-atom bcc Cu supercell and in the bcc Fe matrix

Supercell	Vacancy formation energy (eV)	Previous DFT studies (eV)
Cu cluster	0.73	0.79 [38], 0.71 [42]
Fe matrix	2.27	2.20 [38], 2.02 [39] 2.16 [40], 2.17 [41]

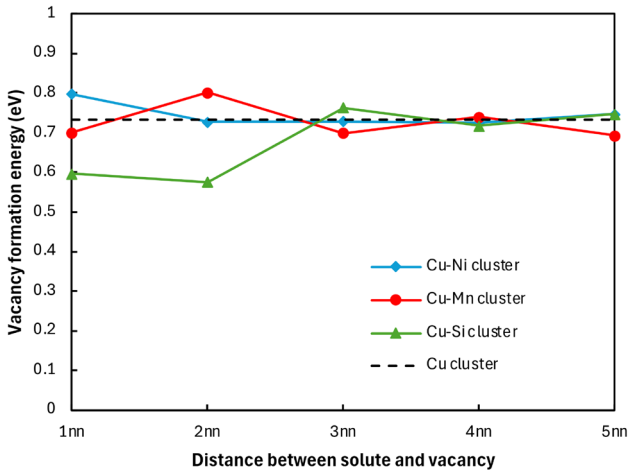

Fig. 2 (Color online) Vacancy formation energies in the solute clusters

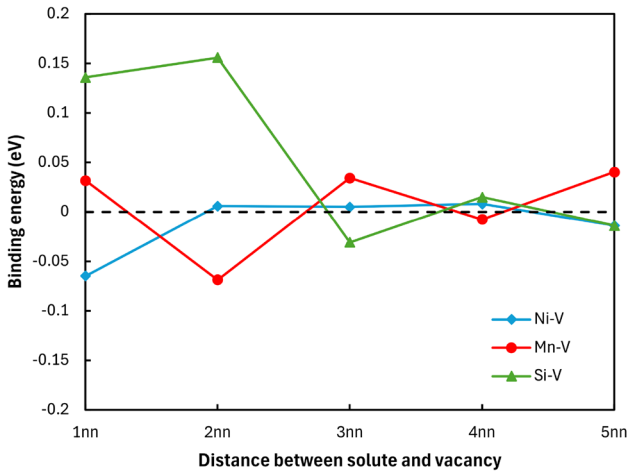

Fig. 3 (Color online) Binding energies between vacancy and solute atom in the solute clusters

consistent with the findings of ab initio calculations because the presence of vacancies between Si and Cu may cause moderate repulsion between Si and Cu and thus reduce the total energy.

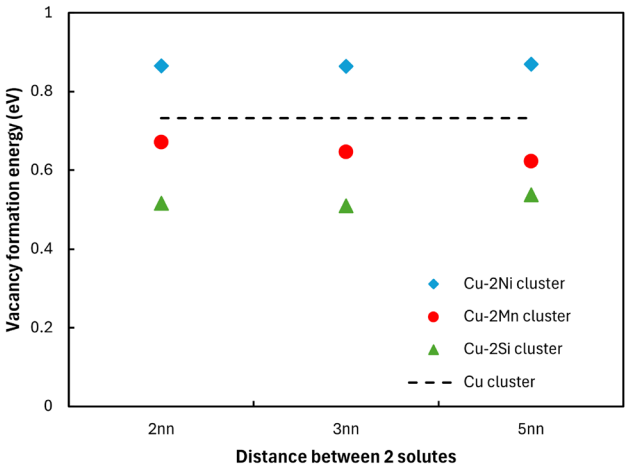

Fig. 4 (Color online) Vacancy formation energies in the solute clusters containing 2 solute atoms

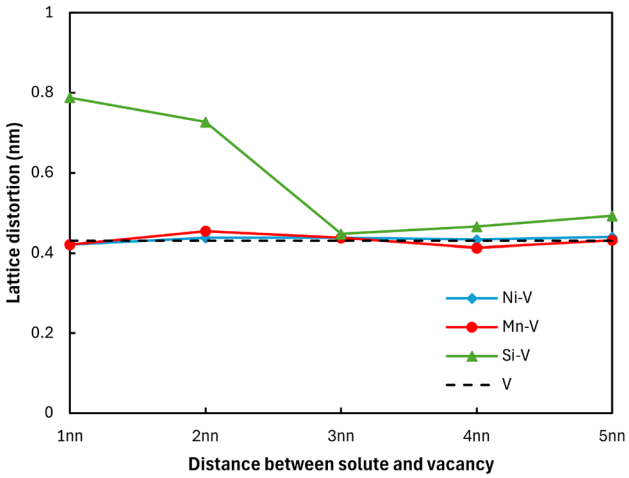

Fig. 5 (Color online) Lattice distortion caused by solute atoms and vacancy in the solute clusters

3.2 Ab initio results for the cluster–matrix interface

A previous atom probe study [22] performed a detailed cluster analysis by obtaining a composition profile across the clusters using the proxigram method. The predominant Cu content was observed inside the cluster, but the Ni, Mn, and Si contents were highest at the cluster–matrix interface. The interface was dominated by the Fe environment. In this study, to better understand the migration behavior of vacancies from the Fe matrix to the solute cluster across the interface, ab initio calculations of solute–vacancy interactions at the cluster–matrix interface were performed. The configuration of the interface was built using a method similar to that in a previous study on solute clusters (see Fig. 1). The vacancy formation energies at the interfaces containing Cu,

Ni, Mn, or Si are shown in Fig. 6. The vacancy formation energies at the interface with one solute atom are lower than those in the Fe matrix when the vacancies are at 1nn and 2nn from the solute atom. When the distance between the solute atom and vacancy is 1nn, it is 0.21 eV, 0.06 eV, 0.13 eV, and 0.26 eV lower at the Fe-Cu, Fe-Ni, Fe-Mn, and Fe-Si interfaces, respectively, than those in the Fe matrix. These results indicate that Cu, Ni, Mn, and Si favor vacancy migration into the solute cluster across the interface. The vacancy formation energies at the interface were close to those in the Fe matrix when the solute–vacancy distance became larger than 3nn, suggesting that these solute–vacancy interactions were short range, which agreed with a previous ab initio study [32]. The binding energies between solute atoms and vacancies at the interfaces are shown in Fig. 7, which corroborates the calculated vacancy formation energies. The results indicated that the Ni-vacancy binding energy was high only at 2nn (0.19 eV); this larger 2nn Ni-vacancy interaction was also observed in previous studies [32, 45, 46]. The binding energies between Cu, Ni, Mn, and Si and the vacancies were positive when the solute–vacancy distance was 5nn. Similar results were obtained by Messina et al. [32]. Olsson et al. [27] suggested that the larger 5nn binding energies were due to Friedel-like relaxation around the vacancies, which led to periodic oscillations in the lattice structure.

The effects of increasing the number of solute atoms at the cluster–matrix interface were investigated. The supercells were constructed by replacing the three Fe atoms with two solute atoms (Ni, Mn, or Si) and one vacancy. This configuration is shown in Fig. 1. Figure 8 presents the vacancy formation energies at the interfaces. The vacancy formation energies at the Fe-2Ni, Fe-2Mn, and Fe-2Si interfaces are lower than the 1nn results at the Fe-Ni, Fe-Mn, and Fe-Si interfaces. This indicates that increasing the number of solute atoms can enhance solute–vacancy interactions at the cluster–matrix interface.

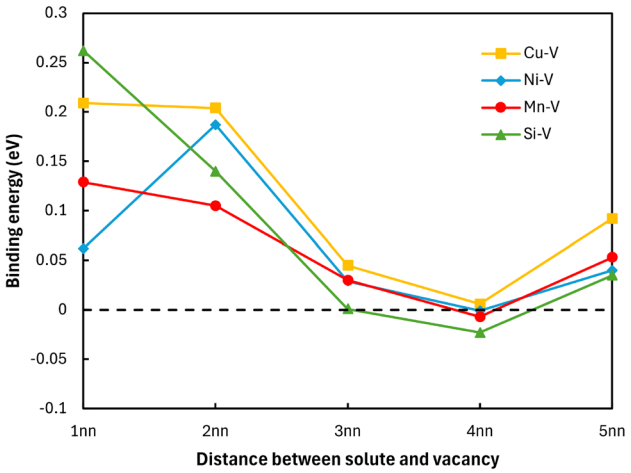

Fig. 7 (Color online) Binding energies between vacancy and solute atom at the cluster–matrix interface

The lattice distortion caused by the solutes and vacancies at the cluster–matrix interface is shown in Fig. 9. In addition, the size effect alone does not suffice as a parameter to comprehend the interactions between solute atoms and vacancies, and the chemical interaction contributes significantly. The results related to Cu, Ni, Mn, and Si are in agreement with those of positron annihilation experiments [28, 47], which show an attractive interaction between the solute and vacancies. The interaction between Mn and the vacancies can be attributed to the magnetism of Mn, as detailed in Sect. 4.1.

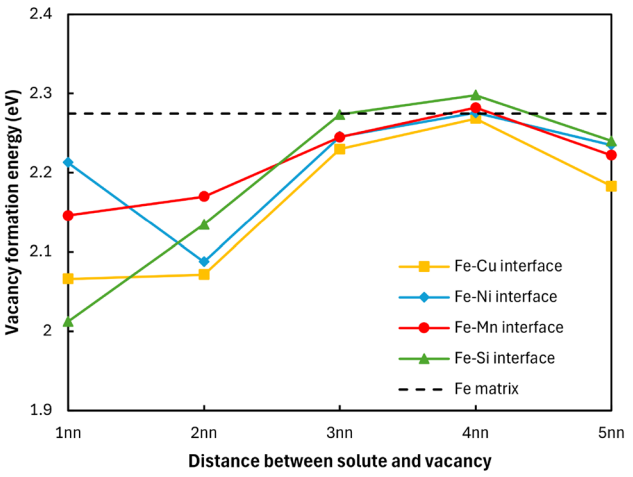

Fig. 6 (Color online) Vacancy formation energies at the cluster–matrix interface

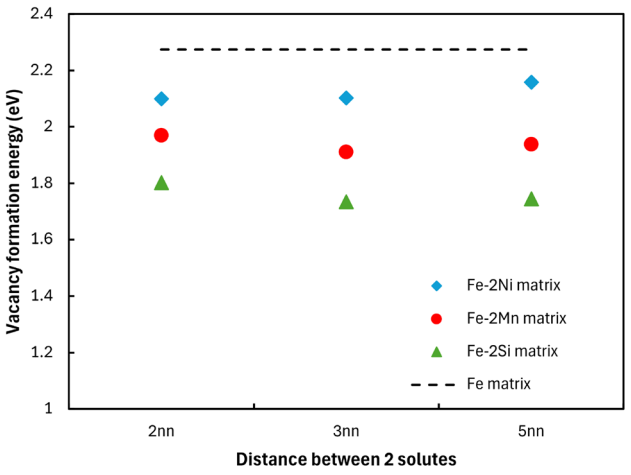

Fig. 8 (Color online) Vacancy formation energies at the cluster–matrix interface containing 2 solute atoms

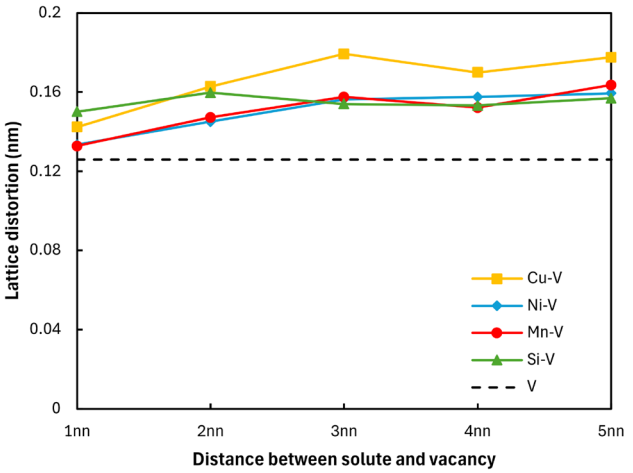

Fig. 9 (Color online) Lattice distortion caused by solute atoms and vacancy at the cluster–matrix interface

Table 2 Local magnetic moments of Mn in the Fe matrix

Defects	Distance	Magnetic moment(s) of Mn (μ_B)
1 Mn	/	−2.44
1 Mn, 1 V	Mn-V 1nn	−2.87
1 Mn, 1 Si	Mn-Si 2nn	−2.56
1 Mn, 1 Si, 1 V	Mn-Si 2nn, Mn-V 1nn	−2.86
1 Mn, 1 Ni	Mn-Ni 2nn	−2.49
1 Mn, 1 Ni, 1 V	Mn-Ni 2nn, Mn-V 1nn	−2.95
2 Mn	Mn-Mn 2nn	−2.37, −2.37
2 Mn, 1 V	Mn-Mn 2nn, Mn-V 1nn	−2.81, −2.81
2 Mn	Mn-Mn 3nn	−2.40, −2.40
2 Mn, 1 V	Mn-Mn 3nn, Mn-V 1nn	−2.90, −2.90
2 Mn	Mn-Mn 5nn	−2.46, −2.46
2 Mn, 1 V	Mn-Mn 5nn, Mn-V 1nn	−2.88, −2.88

4 Discussion

4.1 Effect of magnetic state of Mn

The magnetic moments of Mn atoms in the Fe matrix are listed in Table 2. Mn can be in the ferromagnetic (FM) or antiferromagnetic (AFM) state. In the Fe matrix containing one Mn atom, the magnetic moment of Mn was negative, corresponding to an AFM state. This result is in agreement with that of a previous study [48], in which the calculated energy of an Fe matrix containing one Mn atom reveals that Mn in the AFM state corresponds to a lower substitutional energy; therefore, the AFM state is the ground state of Mn. Table 2 shows that after the addition of a second Mn atom, irrespective of the distance between the two Mn atoms (2nn, 3nn, or 5nn), their magnetic moments are negative ($-2.50 \pm 0.30\ \mu_B$). This result agrees well with the ab initio results reported by Schneider et al. [49], whose investigations show that two Mn atoms with a distance of 1nn or 2nn show antiferromagnetism. These findings are consistent with Radhakrishna et al. [50], who investigated the magnetism of Mn using diffuse neutron scattering in FeMn alloys with different Mn contents (3.15 at%, 5.89 at%, 8.83 at%). They found that the magnetic moments of Mn in the Fe matrix with varying Mn content were always $0.8 \pm 0.1\ \mu_B$, indicating that the magnetic moments of Mn were independent of the number of Mn atoms. In addition, when one Ni or Si atom was close to the Mn atom, the Mn remained in AFM state, indicating that the solute atoms had little effect on the magnetism of the Mn atoms. Notably, when two Mn atoms are in close proximity (2nn), the energy of the supercell with AFM-AFM Mn atoms is only 0.05 eV lower than that with FM-AFM Mn atoms, which may result in the convergence of ab initio calculations to the FM-AFM state. However, after introducing one vacancy, the energy difference increased to 0.27 eV. A previous ab initio study [49] observed that the energy of a 128-atom Fe matrix containing one AFM Mn was lower than that with one FM Mn system by 0.05 eV and increased to 0.28 eV when one vacancy was introduced at the 1nn position of Mn. Considering the vacancy defects in RPV materials, the computational results suggest that Mn in the Fe matrix should be in AFM state. According to Fig. 7, the binding energy of 1nn Mn vacancy in the Fe matrix is 0.13 eV, indicating a short-range attraction between AFM Mn and vacancies. Chen et al. [51] calculated the binding energies between Mn and vacancy clusters V_x ($x \leq 6$) in an Fe matrix, and found that only Mn in AFM state attracted vacancies, which is consistent with the results of this study. This implies that only the AFM state of Mn at the cluster–matrix interface can facilitate vacancy attraction.

Table 3 lists the magnetic moments of the Mn atoms in the solute clusters. A comparison with the results shown in Table 2 demonstrates that after the Fe environment is replaced by the Cu environment, the magnetic states of the Mn atoms change from AFM to FM. This result indicates that the FM state of Mn in the solute clusters is the ground state, and the magnetic moments of Mn are influenced by the surrounding chemical environment. Even after adding another solute atom (Ni or Si), the magnetic moment of Mn remains positive, suggesting a minor influence of nearby solute atoms on the magnetic state of Mn. Additionally, in the solute clusters with two Mn atoms, regardless of the distance between the two Mn atoms (2nn, 3nn, or 5nn), the magnetic moments of Mn persist within the range of $3.55 - 3.66\ \mu_B$, indicating that the magnetism of Mn

Table 3 Local magnetic moments of Mn in the solute clusters

Defects	Distance	Magnetic moment(s) of Mn (μ_B)
1 Mn	/	3.57
1 Mn, 1 V	Mn-V 1nn	3.66
1 Mn, 1 Si	Mn-Si 2nn	3.56
1 Mn, 1 Si, 1 V	Mn-Si 2nn, Mn-V 1nn	3.59
1 Mn, 1 Ni	Mn-Ni 2nn	3.57
1 Mn, 1 Ni, 1 V	Mn-Ni 2nn, Mn-V 1nn	3.60
2 Mn	Mn-Mn 2nn	3.55, 3.55
2 Mn, 1 V	Mn-Mn 2nn, Mn-V 1nn	3.64, 3.63
2 Mn	Mn-Mn 3nn	3.57, 3.57
2 Mn, 1 V	Mn-Mn 3nn, Mn-V 1nn	3.66, 3.66
2 Mn	Mn-Mn 5nn	3.58, 3.58
2 Mn, 1 V	Mn-Mn 5nn, Mn-V 1nn	3.65, 3.65

Table 4 Solute–vacancy and solute–solute binding energies in the Fe matrix

Case	Binding energies (eV)
E_b(Ni-Mn-V 1nn)	0.18
E_b(NiMn-V 1nn)	0.40
E_b(Ni-Si-V 1nn)	2.09
E_b(NiSi-V 1nn)	0.32
E_b(Mn-Si-V 1nn)	2.13
E_b(MnSi-V 1nn)	0.36
E_b(Ni-Mn 1nn)	−0.28
E_b(Ni-Mn 2nn)	−0.22
E_b(Ni-Si 1nn)	1.93
E_b(Ni-Si 2nn)	1.77
E_b(Mn-Si 1nn)	1.91
E_b(Mn-Si 2nn)	1.77
E_b(Ni-V 1nn)	0.06
E_b(Mn-V 1nn)	0.13
E_b(Si-V 1nn)	0.26

is independent of the number of Mn atoms. The binding energies shown in Fig. 3 indicate that the 1nn Mn-vacancy interaction is weak in the solute clusters, in contrast to the attractive interaction between Mn and the vacancies in the Fe matrix. These results confirm that the magnetic state of Mn atoms can affect their interactions with vacancy defects. In solute clusters, Mn atoms are in the FM state, thus leading to weak interactions between Mn and the vacancies.

4.2 Synergistic effect of Ni and Mn

To investigate possible synergistic effects among Ni, Mn, and Si on vacancy aggregation, two different solute atoms and one vacancy were introduced in the supercell, and the structure is shown in Fig. 1. Table 4 summarizes the binding energies between different solute atoms and between solute atoms and vacancies in the Fe matrix. Evidently, the 1nn and 2nn binding energies between Ni and Mn atoms are −0.28 eV and −0.22 eV, respectively, indicating mutual repulsions. This result is consistent with those of previous ab initio calculations [46, 52] of interactions between Ni and Mn in a 128-atom supercell. This finding suggests that the NiMn structure is unstable in the Fe matrix. However, when one vacancy appears at 1nn of the solute atoms, the binding energy among Ni, Mn, and the vacancy (0.18 eV) indicates a strong attraction among them. This finding is consistent with the calculations of Whiting et al. [53]. Thus, vacancies can stabilize structures containing Ni and Mn. Furthermore, Bonny et al. [33] reported simulations, revealing that the tetrahedral structure of Ni_2Mn_2 is stable. Ab initio calculations by Yu et al. [24] indicated that clusters composed of Ni and Mn are thermodynamically stable, implying the presence of Ni and Mn atoms within the solute clusters. Table 4 shows that the 1nn binding energy of NiMn and the vacancy is 0.40 eV, which is significantly higher than the 1nn Ni-vacancy binding energy (0.06 eV) and the 1nn Mn-vacancy binding energy (0.13 eV). This result suggests that Ni and Mn have synergistic effects in attracting vacancies in the Fe matrix.

For Si, the binding energies of 2nn Ni-Si and 2nn Mn-Si were approximately 1.77 eV, and the Ni-Si-vacancy binding energy and Mn-Si–vacancy binding energies were less than 2.13 eV. Therefore, the interaction between solute atoms contributes the most to the attraction between solute atoms and vacancies. The 1nn NiSi-vacancy and MnSi-vacancy binding energies were 0.32 eV and 0.36 eV, respectively, which are close to the 1nn Si-vacancy binding energy (0.26 eV). Therefore, the attraction of NiSi or MnSi to nearby vacancies was mainly caused by the effect of the Si atom.

Table 5 summarizes the binding energies between the solute atoms and between the solute atoms and vacancies within the solute clusters containing two different solute atoms. The binding energy between Ni and Mn at 1nn distance was 0.09 eV, indicating attractive interaction. The interaction between 2nn Ni and Mn is weak (0.03 eV). However, when a vacancy was introduced at 1nn of solute atoms, the binding energy between Ni, Mn, and the vacancies reached 0.28 eV, suggesting an attraction between Ni, Mn, and the vacancies. This implies that introducing a vacancy significantly enhances the attractive interaction. This result agrees with the previous findings of Odette et al. [54]; they investigated the evolution of cluster nucleation using a theoretical model and found that Ni and Mn had a synergistic effect of mutual enhancement; that is, a higher Mn content promoted the enrichment of Ni in the solute clusters, whereas

Table 5 Solute–vacancy and solute–solute binding energies in the solute clusters

Case	Binding energies (eV)
E_b(Ni-Mn-V 1nn)	0.28
E_b(NiMn-V 1nn)	0.25
E_b(Ni-Si-V 1nn)	0.17
E_b(NiSi-V 1nn)	0.17
E_b(Mn-Si-V 1nn)	0.13
E_b(MnSi-V 1nn)	0.14
E_b(Ni-Mn 1nn)	0.09
E_b(Ni-Mn 2nn)	0.03
E_b(Ni-Si 1nn)	0.17
E_b(Ni-Si 2nn)	0.00
E_b(Mn-Si 1nn)	0.10
E_b(Mn-Si 2nn)	−0.01
E_b(Ni-V 1nn)	−0.07
E_b(Mn-V 1nn)	0.03
E_b(Si-V 1nn)	0.14

an increase in the number of Ni atoms could attract more Mn atoms. Chen et al. [22] performed atom probe tomography analyses of Fe-Cu-Ni-Mn alloys after thermal aging and neutron irradiation. Their results demonstrated that the number of Ni atoms and Mn atoms in solute clusters showed a 1:1 relation, which remained unchanged upon varying the Ni content (0.6–0.8 wt%), indicating a synergistic relationship between Ni and Mn. Table 5 also shows that the binding energy between NiMn and 1nn vacancies is 0.25 eV, which is significantly higher than those of 1nn Ni vacancies (−0.07 eV) and 1nn Mn vacancies (0.03 eV). These results indicate that the contribution of Ni or Mn alone in attracting vacancies is small; however, when Ni and Mn coexist, NiMn can facilitate vacancy aggregation. This result suggests that a synergistic effect between Ni and Mn facilitates vacancy aggregation in the solute clusters.

For Si, the Ni-Si-vacancy binding energy was 0.17 eV, and the Mn-Si-vacancy binding energy was 0.13 eV, indicating their strong attraction. As the 1nn Si vacancy binding energy is relatively high (0.14 eV), this attraction is attributed to the effect of Si. In addition, the binding energies of 1nn NiSi-vacancy (0.17 eV) and 1nn MnSi-vacancy (0.14 eV) were close to those of 1nn Si vacancy. This indicates that the effect of Si, rather than the synergistic effect of Ni-Si or Mn-Si, facilitates vacancy aggregation in solute clusters.

4.3 Implication on irradiation embrittlement

To develop a predictive model for radiation embrittlement, clarifying the physical mechanisms of the solute clusters and dislocation loops is imperative. In this study, we investigated the behavior of vacancies in three environments, i.e., Cu-rich clusters, Fe matrix, and a cluster matrix, using ab initio calculations. The basic idea of the modeling is that the Cu-rich cluster and cluster matrix have higher Ni, Mn, and Si contents than the Fe matrix. According to the vacancy formation energies listed in Table 1, Cu clusters can attract vacancies in the Fe matrix. Nagai et al. [28] observed Cu-V_n clusters ($n \leq 6$) produced by electron irradiation at room temperature in Fe-Cu alloys. Wang et al. [55] and Zhao et al. [56] reported that Cu and vacancies can form complexes in Fe-Cu alloys under proton irradiation. Bergner et al. [57] used the small-angle neutron scattering technique to show that clusters produced by neutron irradiation in Fe-Cu alloys contain approximately 84% Cu and 16% vacancies. Previous simulations [19, 20] revealed that Cu clusters in bcc Fe can attract vacancies and nearby interstitial defects. Hernández-Mayoral et al. [18] suggested that the formation of Cu-vacancy complexes induces the recombination of interstitial atoms and vacancies, leading to a decreased defect concentration, thereby inhibiting the growth of dislocation loops. For Cu-rich clusters containing Ni, Mn, and Si, the effect of Si as well as the synergistic effect of Ni and Mn promote the aggregation of vacancies in the solute clusters. In addition, Cu, Ni, Mn, and Si can promote the migration of vacancies across energy barriers from the cluster–matrix interface into the cluster. This observation suggests that vacancies can migrate from the Fe matrix to the solute clusters and thermodynamically aggregate. Therefore, compared with pure Cu clusters, Cu-rich clusters can further absorb vacancies and interstitial defects, thus reducing the concentration of point defects in the Fe matrix and suppressing the growth of dislocation loops while mitigating the irradiation embrittlement of the material.

In contrast, the irradiation embrittlement caused by Cu clusters is affected by the vacancy content in the clusters. Lambrecht et al. [58] conducted a PAS study on Fe-Cu alloys irradiated with 0.1 dpa neutrons, revealing that the Cu clusters formed in the early stage were the primary cause of irradiation hardening, which then became saturated. Further investigations [59] conducted tensile tests on Fe-Cu alloys after neutron irradiation and observed a decrease in the yield strength under neutron irradiation after the saturation of irradiation hardening. They then used PAS techniques and found that the vacancy content in the Cu clusters increased when irradiated with 0.2 dpa compared with 0.1 dpa, suggesting that an increase in the irradiation dose led to an increase in the vacancy content in the Cu clusters, thus resulting in a decrease in the hardening of the Cu clusters. This indicates that the obstacle strength of Cu clusters to moving dislocations decreases as the vacancy content in the clusters increases, thereby affecting irradiation embrittlement. In this study, it was found that solute elements (Ni, Mn, and Si) in solute clusters can facilitate the migration of vacancies

across the cluster–matrix interface into the clusters, leading to an increase in the vacancy content in the solute clusters and a decrease in the obstacle strength of the clusters to moving dislocations. This feature consequently mitigates irradiation embrittlement of the material.

In addition, Soisson et al. [38] utilized ab initio calculations to obtain simulation parameters and subsequently performed Atomistic Kinetic Monte Carlo (AKMC) simulations on the migration of Cu clusters. They found that Cu clusters containing tens of atoms exhibited high mobility, mainly because of the capture of vacancies by the Cu clusters. Castin et al. [60] conducted AKMC simulations of the annealing process of Fe-Cu alloys and observed that Cu clusters with one vacancy had high mobility, and the recombination of mobile Cu clusters was identified as the primary mechanism of the growth and coarsening of Cu clusters. Jourdan et al. [61] employed MD simulations to study the precipitation of Cu in an Fe matrix and revealed that the introduction of the mobility of Cu clusters into the model accelerated the kinetics of precipitation. Thus, vacancy absorption by the Cu clusters enhances their mobility and accelerates the kinetics of Cu precipitation. Because Cu-rich clusters contain solute atoms (Ni, Mn, and Si) that can facilitate vacancy aggregation in the solute clusters, they can accelerate the kinetics of precipitation and growth of Cu-rich clusters, thereby affecting the irradiation embrittlement of high-Cu alloys.

5 Conclusion

Ab initio calculations were performed to investigate the aggregation of vacancies across the cluster–matrix interface into solute clusters containing Cu, Ni, Mn, and Si in bcc Fe. The major conclusions are as follows:

1. Si can facilitate vacancy siting in the solute clusters. Increasing the number of solute atoms could enhance the effects of Si. Both size effect and chemical interaction contribute to the attraction between Si and vacancy in solute clusters.
2. Cu, Ni, Mn, and Si can facilitate vacancy migration from the cluster–matrix interface into the solute clusters. Increasing the number of solute atoms could enhance the effects of Ni, Mn, and Si. Both size effect and chemical interaction contribute to the attraction between solute atoms and vacancies in Fe matrix.
3. The ground state of Mn in the solute clusters and Fe matrix are FM and AFM state, respectively. The magnetic state of Mn is independent of the content of Mn and the surrounding solute atoms. The FM state results in the weak effects of Mn on vacancy aggregation in the solute clusters.
4. Ni and Mn showed synergistic effect on facilitating vacancy aggregation in the solute clusters and attracting vacancies in the Fe matrix.
5. The solute clusters can trap vacancies in the Fe matrix, reducing the concentration of point defects, reducing the obstacle strength of the clusters, and accelerating the precipitation and growth of Cu clusters.

Author Contributions All authors contributed to the study conception and design. Conceptualization was performed by Liang Chen, Yao Shen, and Zheng-Cao Li. Preparation, data collection and analysis were performed by Zhao-Yang Yu, Shi-Hua Qiao, Liang Chen, and Ling-Ti Kong. The first draft of the manuscript was written by Zhao-Yang Yu and all authors commented on previous versions of the manuscript. All authors read and approved the final manuscript.

Data Availability The data that support the findings of this study are openly available in Science Data Bank at https://cstr.cn/31253.11.sciencedb.j00186.00982 and https://www.doi.org/10.57760/sciencedb.j00186.00982.

Declarations

Conflict of interest The authors declare that they have no conflict of interest.

References

1. G.R. Odette, T. Yamamoto, T.J. Williams et al., On the history and status of reactor pressure vessel steel ductile to brittle transition temperature shift prediction models. J. Nucl. Mater. **526**, 151863 (2019). https://doi.org/10.1016/j.jnucmat.2019.151863
2. J. Shi, W. Zhao, Y. Wu et al., Evolution of microstructures and hardening property of initial irradiated, post-irradiation annealed and re-irradiated Chinese-type low-Cu reactor pressure vessel steel. J. Nucl. Mater. **523**, 333–341 (2019). https://doi.org/10.1016/j.jnucmat.2019.06.022
3. X. Xiao, Fundamental mechanisms for irradiation-hardening and embrittlement: a review. Metals **9**, 1132 (2019). https://doi.org/10.3390/met9101132
4. Z. Shen, J. Gao, S. Lv et al., OKMC simulation of vacancy-enhanced Cu solute segregation affected by temperature/irradiation in the Fe–Cu system. Nucl. Sci. Tech. **33**, 149 (2022). https://doi.org/10.1007/s41365-022-01122-x
5. Z. Li, L. Chen, Irradiation embrittlement mechanisms and relevant influence factors of nuclear reactor pressure vessel steels. Acta Metall. Sin. **50**, 1285–1293 (2014). https://doi.org/10.11900/0412.1961.2014.00189
6. H. Liu, X. Wang, W. Cui et al., The effect of dislocations on irradiation-induced vacancy-like defects in FeCu alloy and reactor pressure vessel steel. J. Nucl. Mater. **524**, 80–89 (2019). https://doi.org/10.1016/j.jnucmat.2019.06.040
7. M. Chai, W. Lai, Z. Li et al., Radiation damage of 1Cr18Ni9Ti and Zr-Ti-Al alloys due to energetic particle irradiation. Acta Metall. Sin. Engl. Lett. **25**, 29 (2012). https://doi.org/10.11890/1006-7191-121-29
8. R. Wang, C. Xu, X. Liu et al., Microstructural and mechanical studies of reactor pressure vessel steel under proton irradiation. J. Alloys Compd. **581**, 788–792 (2013). https://doi.org/10.1016/j.jallcom.2013.07.149

9. Y. Hu, X. Cao, P. Zhang et al., Effects of thermal aging on Fe ion-irradiated Fe-0.6% Cu alloy investigated by positron annihilation. Nucl. Sci. Tech. **28**, 16 (2017). https://doi.org/10.1007/s41365-016-0172-9
10. L. Chen, Z. Li, L. Liu et al., Study of the effect of Ni on solute clustering in α-Fe. Nucl. Instrum. Meth. Phys. Res. Sect. B **453**, 28–31 (2019). https://doi.org/10.1016/j.nimb.2019.05.077
11. L. Chen, K. Nishida, K. Murakami et al., A model to evaluate the hardening effect of solute clusters in Fe-based alloys. Nucl. Instrum. Meth. Phys. Res. Sect. B **455**, 32–34 (2019). https://doi.org/10.1016/j.nimb.2019.06.022
12. Z. Zhang, C.T. Liu, M. Miller et al., Effects of proton irradiation on nanocluster precipitation in ferritic steel containing FCC alloying additions. Acta Mater. **60**, 3034–3046 (2012). https://doi.org/10.1016/j.actamat.2012.02.008
13. X.M. Bai, H. Ke, Y. Zhang et al., Modeling copper precipitation hardening and embrittlement in a dilute Fe-0.3 at% Cu alloy under neutron irradiation. J. Nucl. Mater. **495**, 442–454 (2017). https://doi.org/10.1016/j.jnucmat.2017.08.042
14. N. Yamashita, M. Iwasaki, K. Dozaki et al., Industry practice for the neutron irradiation embrittlement of reactor pressure vessels in Japan. J. Eng. Gas Turbines Power **132**, 102919 (2010). https://doi.org/10.1115/1.4001057
15. L. Chen, K. Murakami, D. Chen et al., In situ transmission electron microscopy study of growth of dislocation loops in Fe-Ni alloy under ion irradiation. Scr. Mater. **187**, 453–457 (2020). https://doi.org/10.1016/j.scriptamat.2020.06.071
16. Y. Luo, Y. Dong, X. Wang et al., In-situ TEM study of the effect of pre-existing dislocation on loop evolution in 508-III steel during Fe^+ irradiation. J. Nucl. Mater. **559**, 153420 (2022). https://doi.org/10.1016/j.jnucmat.2021.153420
17. Z. Ding, C. Zhang, X. Zhang et al., Post-irradiation annealing behavior of irradiation hardening of China low-Cu RPV steel. Nucl. Mater. Energy **22**, 100727 (2020). https://doi.org/10.1016/j.nme.2020.100727
18. M. Hernández-Mayoral, D. Gómez-Briceño, Transmission electron microscopy study on neutron irradiated pure iron and RPV model alloys. J. Nucl. Mater. **399**, 146–153 (2010). https://doi.org/10.1016/j.jnucmat.2009.11.013
19. A.C. Arokiam, A.V. Barashev, D.J. Bacon et al., Characteristics of the interaction of Cu-rich precipitates with irradiation-produced defects in α-Fe. Philos. Mag. Lett. **85**, 491–501 (2005). https://doi.org/10.1080/09500830500300047
20. A.C. Arokiam, A.V. Barashev, D.J. Bacon et al., Atomic-scale computer simulation study of the interaction of Cu-rich precipitates with irradiation-produced defects in α-Fe. Philos. Mag. **87**, 925–943 (2007). https://doi.org/10.1080/14786430601003908
21. E.D. Eason, G.R. Odette, R.K. Nanstad et al., A physically-based correlation of irradiation-induced transition temperature shifts for RPV steels. J. Nucl. Mater. **433**, 240–254 (2013). https://doi.org/10.1016/j.jnucmat.2012.09.012
22. L. Chen, K. Nishida, K. Murakami et al., Effects of solute elements on microstructural evolution in Fe-based alloys during neutron irradiation following thermal ageing. J. Nucl. Mater. **498**, 259–268 (2018). https://doi.org/10.1016/j.jnucmat.2017.10.026
23. K. Fukuya, Current understanding of radiation-induced degradation in light water reactor structural materials. J. Nucl. Sci. Technol. **50**, 213–254 (2013). https://doi.org/10.1080/00223131.2013.772448
24. L. Yu, H. Guan, J. Tian et al., Formation and stability of the early stage solute and defect clusters in Cu-free ferritic steels during irradiation. J. Nucl. Mater. **557**, 153297 (2021). https://doi.org/10.1016/j.jnucmat.2021.153297
25. J. Xue, S. Jin, R. Hu et al., Ion-irradiation-induced clustering in Fe-Mn-Ni-(Si) steels: nucleation, growth and chemistry evolution. J. Nucl. Mater. **560**, 153477 (2022). https://doi.org/10.1016/j.jnucmat.2021.153477
26. E. Vincent, C.S. Becquart, C. Domain, Ab initio calculations of vacancy interactions with solute atoms in BCC Fe. Nucl. Instrum. Meth. Phys. Res. Sect. B **228**, 137–141 (2005). https://doi.org/10.1016/j.nimb.2004.10.035
27. P. Olsson, T.P.C. Klaver, C. Domain, Ab initio study of solute transition-metal interactions with point defects in bcc Fe. Phys. Rev. B **81**, 054102 (2010). https://doi.org/10.1103/PhysRevB.81.054102
28. Y. Nagai, K. Takadate, Z. Tang et al., Positron annihilation study of vacancy-solute complex evolution in Fe-based alloys. Phys. Rev. B **67**, 224202 (2003). https://doi.org/10.1103/PhysRevB.67.224202
29. L. Chen, Z.C. Li, H. Schut et al., Positron annihilation study of Fe-ion irradiated reactor pressure vessel model alloys. J. Phys. Conf. Ser. **674**, 012012 (2016). https://doi.org/10.1088/1742-6596/674/1/012012
30. L. Wan, L. Chen, Z. Li, Ab initio calculations of interaction between Ni and Si in α-Fe. J. Nucl. Sci. Technol. **58**, 201–206 (2021). https://doi.org/10.1080/00223131.2020.1815606
31. J.P. Perdew, K. Burke, M. Ernzerhof, Generalized gradient approximation made simple. Phys. Rev. Lett. **77**, 3865–3868 (1996). https://doi.org/10.1103/PhysRevLett.77.3865
32. L. Messina, M. Nastar, T. Garnier et al., Exact ab initio transport coefficients in bcc Fe-X ($X =$ Cr , Cu , Mn , Ni , P , Si) dilute alloys. Phys. Rev. B **90**, 104203 (2014). https://doi.org/10.1103/PhysRevB.90.104203
33. G. Bonny, D. Terentyev, A. Bakaev et al., On the thermal stability of late blooming phases in reactor pressure vessel steels: an atomistic study. J. Nucl. Mater. **442**, 282–291 (2013). https://doi.org/10.1016/j.jnucmat.2013.08.018
34. N. Soneda, K. Dohi, K. Nishida et al., Microstructural characterization of RPV materials irradiated to high fluences at high flux. J. ASTM Int. **6**, 1–16 (2009). https://doi.org/10.1520/JAI102128
35. P. Erhart, J. Marian, B. Sadigh, Thermodynamic and mechanical properties of copper precipitates in α-iron from atomistic simulations. Phys. Rev. B **88**, 024116 (2013). https://doi.org/10.1103/PhysRevB.88.024116
36. J. Wang, M. Enomoto, C. Shang, First-principles study on the interfacial segregation at coherent Cu precipitate/Fe matrix interface. Scr. Mater. **185**, 42–46 (2020). https://doi.org/10.1016/j.scriptamat.2020.03.053
37. A.M. Garrett, C.P. Race, Segregation of Ni and Si to coherent bcc Fe-Cu interfaces from density functional theory. J. Nucl. Mater. **556**, 153185 (2021). https://doi.org/10.1016/j.jnucmat.2021.153185
38. F. Soisson, C.C. Fu, Cu-precipitation kinetics in α-Fe from atomistic simulations: vacancy-trapping effects and Cu-cluster mobility. Phys. Rev. B **76**, 214102 (2007). https://doi.org/10.1103/PhysRevB.76.214102
39. C. Domain, C.S. Becquart, Ab initio calculations of defects in Fe and dilute Fe-Cu alloys. Phys. Rev. B **65**, 024103 (2001). https://doi.org/10.1103/PhysRevB.65.024103
40. G. Lucas, R. Schäublin, Vibrational contributions to the stability of point defects in bcc iron: a first-principles study. Nucl. Instrum. Meth. Phys. Res. Sect. B **267**, 3009–3012 (2009). https://doi.org/10.1016/j.nimb.2009.06.110
41. T. Ohnuma, N. Soneda, M. Iwasawa, First-principles calculations of vacancy–solute element interactions in body-centered cubic iron. Acta Mater. **57**, 5947–5955 (2009). https://doi.org/10.1016/j.actamat.2009.08.020
42. K. Sato, T. Ihara, H. Sakurai et al., Comparison of interaction between Cu precipitate and vacancy in Fe using first-principle calculations and empirical N-body potential calculations. Comput.

Mater. Sci. **47**, 521–525 (2009). https://doi.org/10.1016/j.commatsci.2009.09.020
43. K. Fukuya, K. Ohno, H. Nakata et al., Microstructural evolution in medium copper low alloy steels irradiated in a pressurized water reactor and a material test reactor. J. Nucl. Mater. **312**, 163–173 (2003). https://doi.org/10.1016/S0022-3115(02)01675-6
44. N. Soneda, K. Dohi, A. Nomoto et al., Embrittlement correlation method for the Japanese reactor pressure vessel materials. J. ASTM Int. **7**, 1–20 (2010). https://doi.org/10.1520/JAI102127
45. A. Möslang, E. Albert, E. Recknagel et al., Investigation of electron irradiated iron alloys and nickel. Hyperfine Interact. **17**, 255–259 (1984). https://doi.org/10.1007/BF02065911
46. L. Malerba, G.J. Ackland, C.S. Becquart et al., Ab initio calculations and interatomic potentials for iron and iron alloys: achievements within the Perfect Project. J. Nucl. Mater. **406**, 7–18 (2010). https://doi.org/10.1016/j.jnucmat.2010.05.016
47. Y. Nagai, Z. Tang, M. Hassegawa et al., Irradiation-induced Cu aggregations in Fe: an origin of embrittlement of reactor pressure vessel steels. Phys. Rev. B **63**, 134110 (2001). https://doi.org/10.1103/PhysRevB.63.134110
48. D.J.M. King, S.C. Middleburgh, P.A. Burr et al., Density functional theory study of the magnetic moment of solute Mn in bcc Fe. Phys. Rev. B **98**, 024418 (2018). https://doi.org/10.1103/PhysRevB.98.024418
49. A. Schneider, C.C. Fu, C. Barreteau, Local environment dependence of Mn magnetism in bcc iron-manganese alloys: a first-principles study. Phys. Rev. B **98**, 094426 (2018). https://doi.org/10.1103/PhysRevB.98.094426
50. P. Radhakrishna, F. Livet, Environmental effects in iron-manganese alloys. Solid State Commun. **25**, 597–600 (1978). https://doi.org/10.1016/0038-1098(78)91498-9
51. D. Chen, K. Murakami, L. Chen et al., An investigation of nucleation sites for the formation of solute clusters in ferrite Fe. Nucl. Instrum. Meth. Phys. Res. Sect. B **478**, 182–186 (2020). https://doi.org/10.1016/j.nimb.2020.06.037
52. O.I. Gorbatov, A.H. Delandar, Y.N. Gornostyrev et al., First-principles study of interactions between substitutional solutes in bcc iron. J. Nucl. Mater. **475**, 140–148 (2016). https://doi.org/10.1016/j.jnucmat.2016.04.013
53. T.M. Whiting, P.A. Burr, D.J.M. King et al., Understanding the importance of the energetics of Mn, Ni, Cu, Si and vacancy triplet clusters in bcc Fe. J. Appl. Phys. **126**, 115901 (2019). https://doi.org/10.1063/1.5109483
54. G.R. Odette, B.D. Wirth, A computational microscopy study of nanostructural evolution in irradiated pressure vessel steels. J. Nucl. Mater. **251**, 157–171 (1997). https://doi.org/10.1016/S0022-3115(97)00267-5
55. R.S. Wang, X.B. Liu, A. Ren et al., Proton-irradiation-induced damage in Fe-0.3 wt% Cu alloys characterized by positron annihilation and nanoindentation. Nucl. Instrum. Meth. Phys. Res. Sect. B **307**, 545–551 (2013). https://doi.org/10.1016/j.nimb.2012.11.090
56. W. Zhao, J. Shi, Z. Yang et al., Postirradiation annealing and reirradiation study of high-dose proton-irradiated Fe–Cu model alloys by positron annihilation and nanoindentation. Phys. Status Solidi B **258**, 2000458 (2021). https://doi.org/10.1002/pssb.202000458
57. F. Bergner, A. Ulbricht, P. Lindner et al., Post-irradiation annealing behavior of neutron-irradiated FeCu, FeMnNi and FeMnNiCu model alloys investigated by means of small-angle neutron scattering. J. Nucl. Mater. **454**, 22–27 (2014). https://doi.org/10.1016/j.jnucmat.2014.07.038
58. M. Lambrecht, L. Malerba, A. Almazouzi, Influence of different chemical elements on irradiation-induced hardening embrittlement of RPV steels. J. Nucl. Mater. **378**, 282–290 (2008). https://doi.org/10.1016/j.jnucmat.2008.06.030
59. M. Lambrecht, A. Almazouzi, Positron annihilation study of neutron irradiated model alloys and of a reactor pressure vessel steel. J. Nucl. Mater. **385**, 334–338 (2009). https://doi.org/10.1016/j.jnucmat.2008.12.020
60. N. Castin, M.I. Pascuet, L. Malerba, Modeling the first stages of Cu precipitation in α-Fe using a hybrid atomistic kinetic Monte Carlo approach. J. Chem. Phys. **135**, 064502 (2011). https://doi.org/10.1063/1.3622045
61. T. Jourdan, F. Soisson, E. Clouet et al., Influence of cluster mobility on Cu precipitation in α-Fe: a cluster dynamics modeling. Acta Mater. **58**, 3400–3405 (2010). https://doi.org/10.1016/j.actamat.2010.02.014